Article

Stoichiometry and Morphology Analysis of Thermally Deposited V_2O_{5-x} Thin Films for Si/V_2O_{5-x} Heterojunction Solar Cell Applications

Gwan Seung Jeong [1], Yoon-Chae Jung [1], Na Yeon Park [1], Young-Jin Yu [1], Jin Hee Lee [2], Jung Hwa Seo [3] and Jea-Young Choi [4,*]

[1] Department of Metallurgical Engineering, Dong-A University, Busan 49315, Korea; wjdrhkstmd12@gmail.com (G.S.J.); dbsco0306@naver.com (Y.-C.J.); nayeon2385@gmail.com (N.Y.P.); tq6284@naver.com (Y.-J.Y.)
[2] Department of Chemical Engineering, Dong-A University, Busan 49315, Korea; dljh82@gmail.com
[3] Department of Physics, University of Seoul, Seoul 02504, Korea; seojh@uos.ac.kr
[4] Department of Materials Sciences & Engineering, Dong-A University, Busan 49315, Korea
* Correspondence: cjy4395@dau.ac.kr

Abstract: In recent decades, dopant-free Si-based solar cells with a transition metal oxide layer have gained noticeable research interest as promising candidates for next-generation solar cells with both low manufacturing cost and high power conversion efficiency. Here, we report the effect of the substrate temperature for the deposition of vanadium oxide (V_2O_{5-x}, $0 \leq X \leq 5$) thin films (TFs) for enhanced Si surface passivation. The effectiveness of SiO_x formation at the Si/V_2O_{5-x} interface for Si surface passivation was investigated by comparing the results of minority carrier lifetime measurements, X-ray photoelectron spectroscopy, and atomic force microscopy. We successfully demonstrated that the deposition temperature of V_2O_{5-x} has a decisive effect on the surface passivation performance. The results confirmed that the aspect ratio of the V_2O_{5-x} islands that are initially deposited is a crucial factor to facilitate the transport of oxygen atoms originating from the V_2O_{5-x} being deposited to the Si surface. In addition, the stoichiometry of V_2O_{5-x} TFs can be notably altered by substrate temperature during deposition. As a result, experimentation with the fabricated Si/V_2O_{5-x} heterojunction solar cells confirmed that the power conversion efficiency is the highest at a V_2O_{5-x} deposition temperature of 75 °C.

Keywords: transition metal oxide; vanadium oxide; passivation; heterojunction solar cell

Citation: Jeong, G.S.; Jung, Y.-C.; Park, N.Y.; Yu, Y.-J.; Lee, J.H.; Seo, J.H.; Choi, J.-Y. Stoichiometry and Morphology Analysis of Thermally Deposited V_2O_{5-x} Thin Films for Si/V_2O_{5-x} Heterojunction Solar Cell Applications. *Materials* **2022**, *15*, 5243. https://doi.org/10.3390/ma15155243

Academic Editor: Ji-Woong Kim

Received: 7 July 2022
Accepted: 27 July 2022
Published: 29 July 2022

Publisher's Note: MDPI stays neutral with regard to jurisdictional claims in published maps and institutional affiliations.

Copyright: © 2022 by the authors. Licensee MDPI, Basel, Switzerland. This article is an open access article distributed under the terms and conditions of the Creative Commons Attribution (CC BY) license (https://creativecommons.org/licenses/by/4.0/).

1. Introduction

Crystalline Si (c-Si) solar cells are considered to be promising next-generation energy providers as one of the most mature technologies in the renewable energy market. However, from an economic viewpoint, c-Si solar cells are still inferior to existing energy sources based on fossil fuel. Consequently, much work remains to be done to drastically increase their market share, keeping in mind the pressing issue of global warming. The low economic feasibility of existing c-Si solar cells is primarily attributable to following factors: (1) their excessive consumption of materials (e.g., Si) and (2) relatively complicated and high-temperature fabrication process. Therefore, various cost-saving technologies have recently been explored. One representative technology is the production of solar cells using a thin Si wafer (<50 μm) to reduce the required amount of Si (i.e., the material that accounts for more than 40% of the cost of manufacturing a solar cell module) [1]. This technology is able to considerably lower the cost of materials for solar cell production. However, because Si has a low absorption coefficient in the long-wavelength region [2,3], the amount of light absorbed by a Si absorber with a reduced thickness also decreases. This, in turn, lowers the power conversion efficiency (PCE) of the solar cells [4,5]. Attempts to address this shortcoming

have resulted in the exploration of various technologies to improve the productivity while simplifying the manufacturing process. A possible approach to overcome these problems includes the introduction of novel materials which would enable the development of low-cost and high-efficiency solar cells after combining with c-Si. Thanks to these efforts, many novel materials with distinct optical and electrical characteristics such as perovskite [6,7], organic polymers [8,9], transparent conductive oxides [10], and transition metal oxides (TMOs) [11,12] have been developed. Recently, many researchers also actively investigated the realistic application of these materials to fabricate c-Si-based heterojunction solar cells (Si-HSCs), which could minimize the cost issue stemming from complicated and high-temperature fabrication processes such as the thermally diffused doping process to build a PN junction in a conventional c-Si-based solar cell [13,14].

Among them, TMOs (e.g., V_2O_5, MoO_3, WO_3, and TiO_2) are useful as excellent carrier-selective hetero-contact materials for n-type and p-type Si, both of which have work functions with a wide energy range (Φ_{TMO} = 3~7 eV), as shown in Figure 1 [15,16]. They also offer excellent window layer characteristics that can minimize the decrease in PCE resulting from the parasitic absorption by the front layers of solar cells because of their large energy band gap (E_g > 3 eV) [17–19]. In addition, TMOs are promising for reducing the processing cost, as the layers can be formed via low-cost processes such as evaporation (e.g., thermal and electron-beam) or spin coating [20–22]. Recently, a high PCE of 22.5% was achieved using a Si/TMO HSC in which TMOs (e.g., V_2O_5, MoO_3, and WO_3) were employed as the hole-selective contact layer. This promising achievement demonstrates the high potential of Si/TMO HSCs as low-cost next-generation solar cells capable of yielding high efficiency [23].

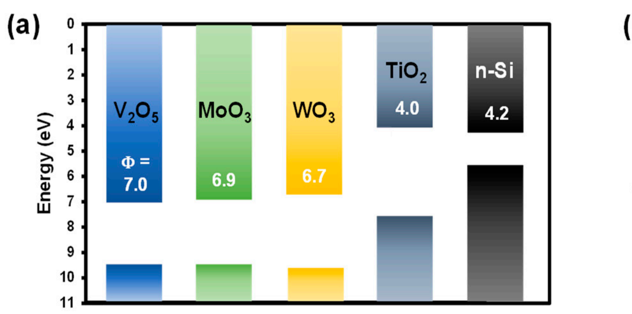

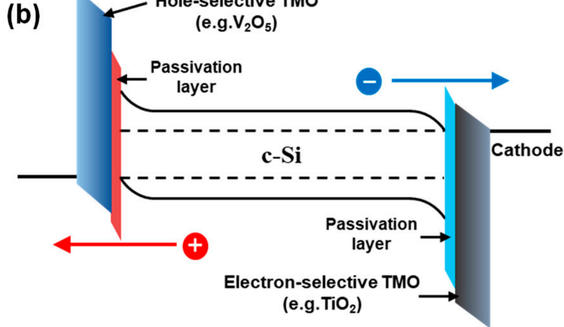

Figure 1. (**a**) Reported work functions (Φ) for TMOs (V_2O_5, MoO_3, WO_3, and TiO_2) and (**b**) energy band diagram with electron- and hole-selective contacts for c-Si/TMO HSCs.

Despite the aforementioned advantages, the carrier recombination velocity at the Si/TMO interface created by depositing the TMOs is generally high. This situation arises because of the incomplete formation of the silicon dioxide (SiO_2) layer, which acts as a passivation layer for the Si surface, at the low temperatures at which the TMOs are processed. The resulting short lifetime of the photo-generated carriers lowers the PCE of the solar cell [24]. The development of a method that would enable the formation of high-quality passivation layers for the Si surface in the form of a TMO deposition is, therefore, essential to fabricate high-efficiency Si/TMO HSCs.

In this study, we firstly investigated the deposition temperature effect of TMO, specifically vanadium oxide (V_2O_{5-x}), to form a SiO_y ($0 \leq y \leq 2$) passivation layer for Si surfaces. In many previous reports, the passivation effect of TMO for Si surfaces was studied, but they mostly focused on comparisons between different kinds of TMO such as V_2O_5, MoO_3, and WO_3, or high-temperature post-thermal annealing effects after TMO deposition [25,26]. In this report, V_2O_{5-x} was deposited at various Si substrate temperatures below 150 °C. Subsequently, the (1) stoichiometry, (2) morphology, and (3) Si surface passivation capability of the deposited V_2O_{5-x} thin films (TFs) were investigated. Our results clearly revealed that the passivation characteristics of the Si surface could be noticeably improved

by adjusting the temperature of the Si substrate, i.e., the deposition temperature, but that the temperature had to remain below 100 °C for the thermal deposition of V_2O_{5-x}.

The effect of the V_2O_{5-x} deposition temperature on the PCE of the Si/V_2O_{5-x} HSC was evaluated by fabricating Si/V_2O_{5-x} HSCs at different substrate temperatures. The HSC with the most enhanced PCE was fabricated at a deposition temperature of 75 °C, and this PCE was 25% higher than that of the sample that was not heated during the deposition. These results demonstrated that high-efficiency Si/TMO HSCs could potentially be fabricated by simply making a minor adjustment to the process temperature for TMO deposition.

2. Experimental

2.1. Materials and Sample Preparation

A double-sided polished n-type CZ silicon wafer with a (100) orientation, thickness of 280 µm, and resistivity of 1.7–2.3 Ω-cm was cut to a size of 2 × 2 cm. The wafer was cleaned by sequential ultra-sonication with acetone, methanol, and distilled water (DI water) for 15 min each. Subsequent standard RCA cleaning with a mixture of NH_4OH, H_2O_2, and DI water at a volume ratio of 1:1:5 served to remove residual organic contaminants from the wafer surface. The native oxides on the Si surface were removed by immersion in dilute HF (1 vol.%) for 1 min. The V_2O_{5-x} TF (V_2O_5 powder, 99.99%, Sigma Aldrich, St. Louis, MI, USA) was thermally deposited at 0.2 Å/s at various substrate temperatures (no heating, 50, 75, 100, and 125 °C) at a vacuum level of ~1.0×10^{-6} mbar.

Four different sample structures were fabricated in this study. The first was a V_2O_{5-x} (15 nm)/n-Si/V_2O_{5-x} (15 nm) sample structure for measuring the minority carrier lifetime (τ_{eff}); the second was a Ag (200 nm)/V_2O_{5-x} (15 nm)/n-Si structure with grid contact for measuring the sheet resistance via the transmission line method (TLM); the third was a V_2O_{5-x} (5 nm and 15 nm)/n-Si structure for analyzing the surface morphology and XPS characteristics of the V_2O_{5-x} TF; and the fourth was a Ag (200 nm)/V_2O_{5-x} (15 nm)/n-Si/Al (200 nm) structure for measuring the built-in potential (V_{bi}).

2.2. Characterization

The dependence of τ_{eff} on the V_2O_{5-x} deposition temperature was analyzed by measuring the τ_{eff} with a photo-conductance decay system (WCT-120, Sinton Instrument Inc., Boulder, CO, USA). The surface morphology of the deposited V_2O_{5-x} TF was examined by acquiring atomic force microscopy (AFM) images in the tapping mode (Veeco Multi-Mode-V). The changes in the compositions of the V_2O_{5-x} and the formed SiO_x layers arising from oxidation and reduction reactions between the deposited V_2O_{5-x} TF and the Si surface were studied using X-ray photoelectron spectroscopy (XPS, ESCALAB 250XI, Thermo-Fisher, Waltham, MA, USA). The conductivity of the V_2O_{5-x} TF was derived using the sheet resistance measured via the TLM. V_{bi} was obtained by measuring the capacitance–voltage (C–V) relationship using the Agilent E4980A LCR meter. Finally, the PCE of the fabricated HSCs was measured under the simulated air mass (AM) 1.5G condition after calibration using a standard silicon reference cell.

3. Results and Discussion

In preparation for the τ_{eff} measurements to assess the effect of the V_2O_{5-x} deposition temperature on the Si surface passivation, samples were fabricated as a sandwich structure by depositing V_2O_{5-x} on both sides of the Si substrate at the following deposition temperatures: RT (i.e., no heating), 50, 75, 100, and 125 °C. The results are shown in Figure 2.

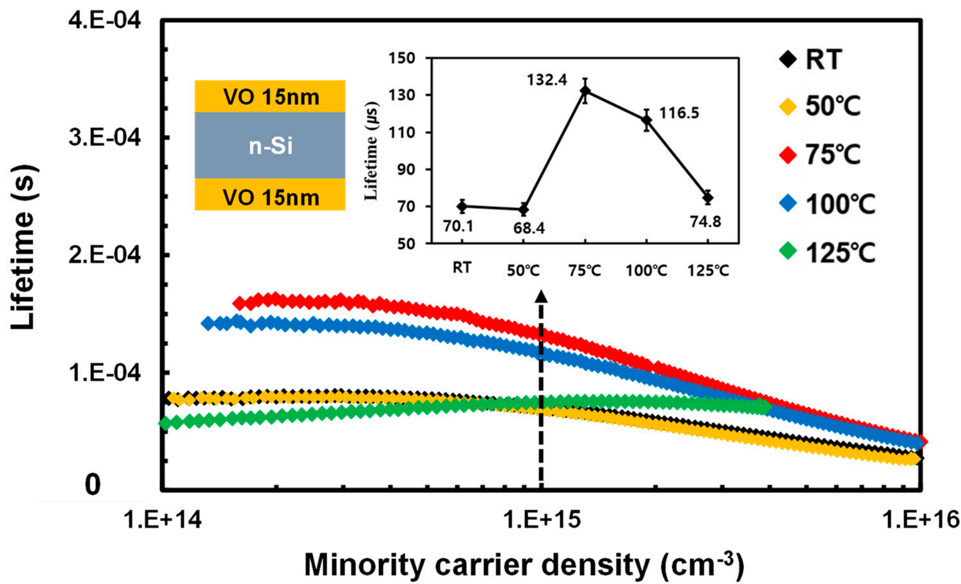

Figure 2. Minority carrier lifetimes plotted against the minority carrier density. Carrier lifetimes were measured at different V_2O_{5-x} deposition temperatures for the cell structure in the inset. (Note: The vertical black dashed arrow indicates the carrier injection level of 1.5×10^{15} cm^{-3} at which the τ_{eff} values in the inset were derived).

As shown in Figure 2, the τ_{eff} values of the samples measured at RT and 50 °C were comparable at 70 µs and 68 µs, respectively. However, at 75 °C, the τ_{eff} dramatically increased to 132 µs. In contrast, the samples at 100 °C and 125 °C had τ_{eff} values of 116 µs and 75 µs, respectively, indicating a decreasing trend at deposition temperatures beyond 75 °C. This result implies that the passivation effect of the V_2O_{5-x} TF can be altered by adjusting the deposition temperature, and that effective passivation was possible even at temperatures below 100 °C. Most importantly, this result reveals the existence of a specific deposition temperature at which the passivation effect is significantly enhanced. The improved Si surface passivation effect is expected to lead to a high short-circuit current (J_{SC}) and open-circuit voltage (V_{OC}), by decreasing the reverse saturation current (J_0) when actual Si/TMO HSCs are fabricated [27]. According to a previous study, the Si surface passivation effect of a deposited V_2O_{5-x} TF arises from the formation of a SiO_x layer at the V_2O_{5-x}/Si interface when the oxygen atoms in V_2O_{5-x} migrate to the Si surface during V_2O_{5-x} deposition [28]. This migration of oxygen (O) atoms to the Si surface originates from the more negative Gibbs formation energy (ΔG) for SiO_2 compared to that of V_2O_{5-x}. This is evident from the following chemical formula and the change in the Gibbs free energy (ΔG_{Si-O_2}) [25,29].

$$\frac{5}{2}\mathrm{Si} + \frac{5}{2}\mathrm{O_2} \rightarrow \frac{5}{2}\mathrm{SiO_2} \qquad \Delta G_{Si-O_2} = -858\ \mathrm{kJ/mol}$$

$$2\mathrm{V} + \frac{5}{2}\mathrm{O_2} \rightarrow \mathrm{V_2O_5} \qquad \Delta G_{V-O_2} = -573\ \mathrm{kJ/mol}$$

Therefore, when V_2O_{5-x} is deposited on the Si surface, the migration of the O atoms in the V_2O_{5-x} TF to the Si surface for SiO_2 formation is induced by the negative $\Delta G_{Si-V_2O_5}$ (−285 kJ/mol), as shown below.

$$\frac{5}{2}\mathrm{Si} + \mathrm{V_2O_5} \rightarrow \frac{5}{2}\mathrm{SiO_2} + 2\mathrm{V}$$

$$\Delta G_{Si-V_2O_5} = \Delta G_{Si-O_2} - \Delta G_{V-O_2} = -285\ \mathrm{kJ/mol}$$

However, the spontaneity of this thermodynamic reaction would be expected to increase when the temperature increases [30]. This led us to predict that, in our study, an increase in the V_2O_{5-x} deposition temperature would lead to a gradual increase in τ_{eff} owing to the formation of SiO_y ($0 \leq y \leq 2$) on the Si surface. However, as shown in Figure 2, τ_{eff} increased until 75 °C, above which it decreased again at the higher temperatures of 100 °C and 125 °C. Therefore, the XPS profiles of these samples were measured to study the effect of the deposition temperature on the formation of the SiO_y passivation layer at the V_2O_{5-x}/Si interface. The Si 2p XPS profiles, shown in Figure 3, are the Gaussian profiles, which were deconvoluted to reveal peaks for the Si substrate (Si^0, 99.2 eV), sub-stoichiometric SiO_z (Si^{1+}~100.15 eV, Si^{2+}~101.05 eV, Si^{3+}~101.75 eV), and stoichiometric SiO_2 (Si^{4+}~103.15 eV) [31,32]. This enabled the ratios of Si^0, SiO_z, and SiO_2 at the Si/V_2O_{5-x} interface to be determined according to the deposition temperature by integrating the area of each separated peak. The ratio change between Si^0 and SiO_y with deposition temperature is presented in Figure 4; the detail ratios are also listed in the embedded table.

As is evident from the embedded table in Figure 4, when the temperature was increased from RT to 75 °C, the ratio of Si^0 decreased from 11% to 4%, but those of SiO_z and SiO_2 increased. The ratio of SiO_2 (i.e., Si^{4+}) increased particularly at 75 °C, confirming the formation of the highest quality SiO_y passivation layer at 75 °C compared to those at RT and 50 °C. However, the increase in the SiO_2 ratio is small compared to that at 75 °C, whereas the increase in the Si^0 ratio is observed to be significant; consequently, at 100 °C, the total SiO_y (i.e., sum ratio of $SiO_{z\sim1.5}$ and SiO_2) formation ratio decreased as shown in Figure 4. At 125 °C, the further decrease in the total SiO_y ratio is mainly attributed to the reduced ratio of SiO_2.

Based on the Si 2p XPS profiles, the deposition temperature has a marked influence on the V_2O_{5-x} passivation effect, even below 100 °C. However, as was previously reported, TMOs are well known to require relatively high deposition temperatures (>400 °C) to thermally induce the effective reduction of the TMOs to form SiO_y on the Si surface [26,33]. Therefore, we assume that the enhanced passivation effect we observed in our work at such a low temperature most probably had morphological origins rather than the TMO reduction being facilitated by temperature. To confirm our assumption, the initially deposited 5 nm thick $V2O_{5-x}$ layer was analyzed by AFM to study the morphological change at different deposition temperatures.

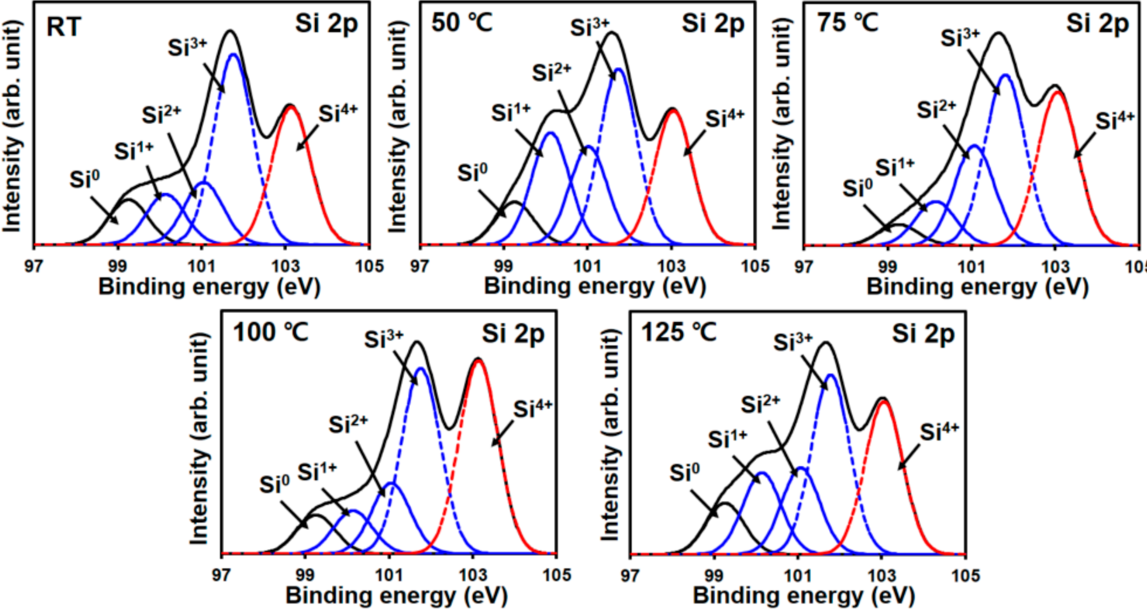

Figure 3. Si 2p spectra of SiO_y formed at the V_2O_{5-x} (15 nm)/Si interfaces at each of the different temperatures.

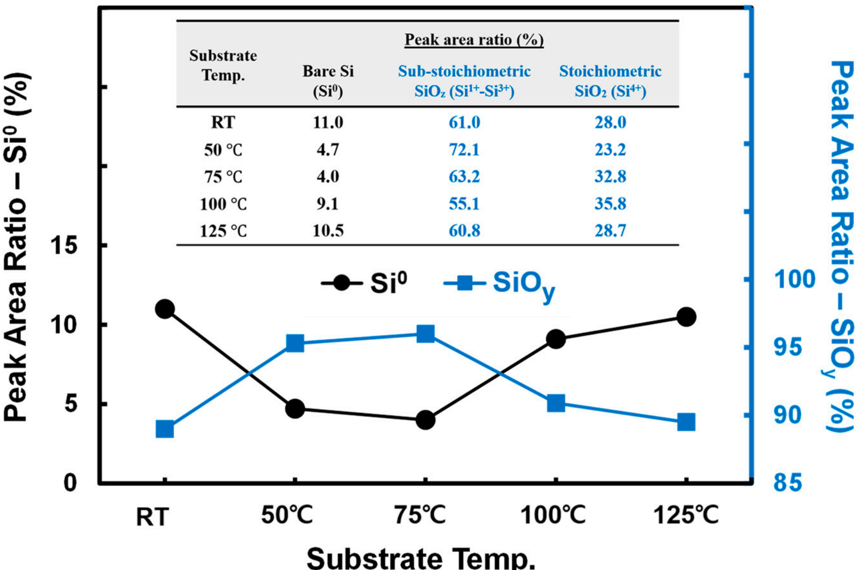

Substrate Temp.	Peak area ratio (%)		
	Bare Si (Si^0)	Sub-stoichiometric SiO_z (Si^{1+}-Si^{3+})	Stoichiometric SiO_2 (Si^{4+})
RT	11.0	61.0	28.0
50 °C	4.7	72.1	23.2
75 °C	4.0	63.2	32.8
100 °C	9.1	55.1	35.8
125 °C	10.5	60.8	28.7

Figure 4. Peak area ratios of Si states calculated by measured Si 2p doublet spectra.

The AFM results (Figure 5) indicated that the deposited V_2O_{5-x} of 5 nm thickness produced isolated islands. Before obtaining the AFM results, we actually expected that the surface coverage of these V_2O_{5-x} islands would continue to increase with the substrate temperature because the temperatures at which we conducted the measurements were in the low-temperature regime [34–36]. However, as shown in Figure 5f, the surface coverage by V_2O_{5-x} increased only until 75 °C, above which the islands again became more distinct. The uniformity of the V_2O_{5-x} islands also followed this trend of coverage and revealed the lowest root mean square roughness (RMS) at 75 °C. Based on these AFM results, we confirmed that, even in this low-temperature regime, the morphology of the V_2O_{5-x} TF was significantly affected.

Based on this morphological sensitivity of the initial V_2O_{5-x} islands to the deposition temperature, we surmised that the formation of the SiO_x passivation layer at the V_2O_{5-x}/Si interface was mainly influenced by the V_2O_{5-x} morphology. To clarify our theory, we further investigated the change in the V_2O_{5-x} morphology in terms of the aspect ratio (AR) of the initial V_2O_{5-x} islands. Figure 6a–e shows the height (H) and width (W) of the V_2O_{5-x} islands measured from the cross-sectional profiles of the AFM images to derive their AR at the different deposition temperatures. The obtained ARs are plotted in Figure 6f; this graph shows that the V_2O_{5-x} islands formed at 75 °C had the lowest AR, 0.093, compared to those for the other temperatures. The advantage of such a low AR is that it can offer an expanded active region for supplying O atoms to the Si surface compared to those with higher ARs for the same amount of deposited V_2O_{5-x} (Figure 6g,h). Therefore, a lower AR would be expected to result in the formation of a more effective SiO_y passivation layer over a larger Si surface resulting from V_2O_{5-x} deposition.

A possible mechanism whereby the thermally evaporated atoms are deposited is illustrated in Figure 7 as an attempt to explain the variation in the AR with the deposition temperature. Accordingly, the formation of the V_2O_{5-x} TF occurs in five steps: (a) First, the solid-state V_2O_{5-x} in the evaporation boat is decomposed into V and O atoms, respectively, in the vapor state during thermal deposition and (b) these atoms diffuse to the substrate. (c) As soon as the atoms reach the substrate, the substrate induces thermal energy (TE) loss, and the atoms are converted to the liquid state and wetted (or adsorbed) onto the substrate. (d) Then, the atoms are transported across the surface for nucleation of the V_2O_{5-x} with the residual TE. (e) Finally, a continuous V_2O_{5-x} TF is grown with the subsequent supply of V and O atoms [37,38].

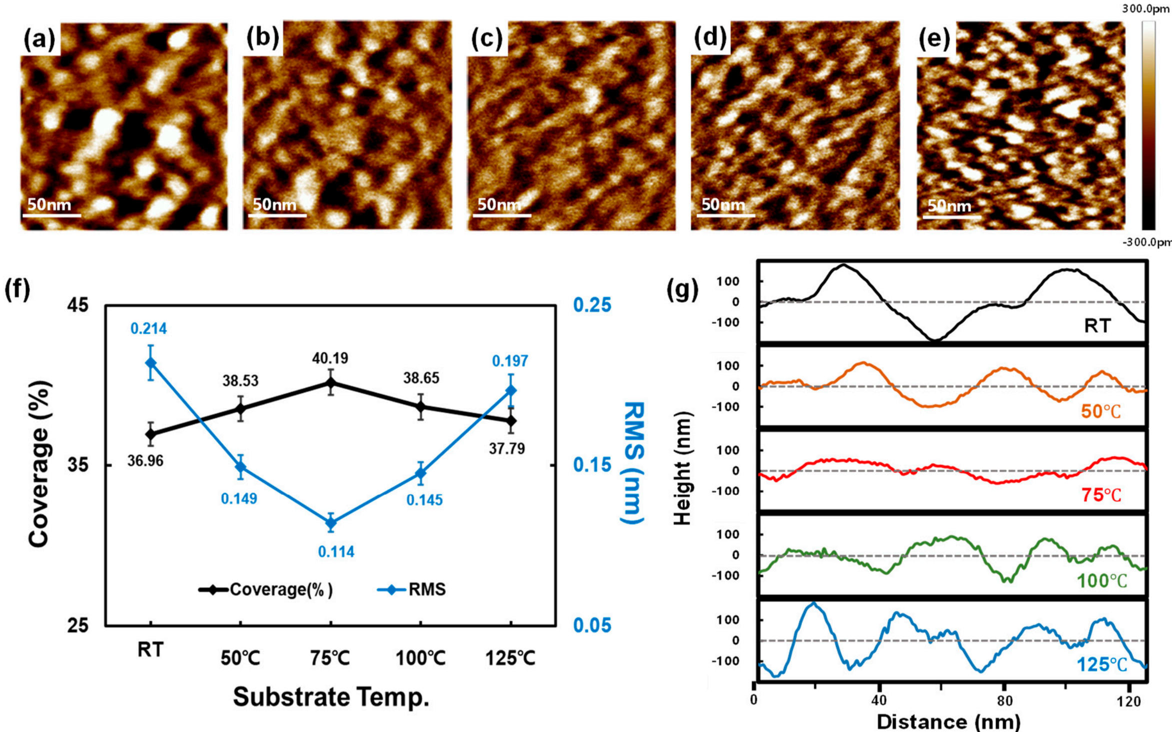

Figure 5. AFM image of V_2O_{5-x} (5 nm) TF deposited at different substrate temperatures: (**a**) RT, (**b**) 50 °C, (**c**) 75 °C, (**d**) 100 °C, and (**e**) 125 °C. (**f**) Surface coverage and roughness (RMS) and (**g**) cross-sectional profile of each deposited V_2O_{5-x} TF.

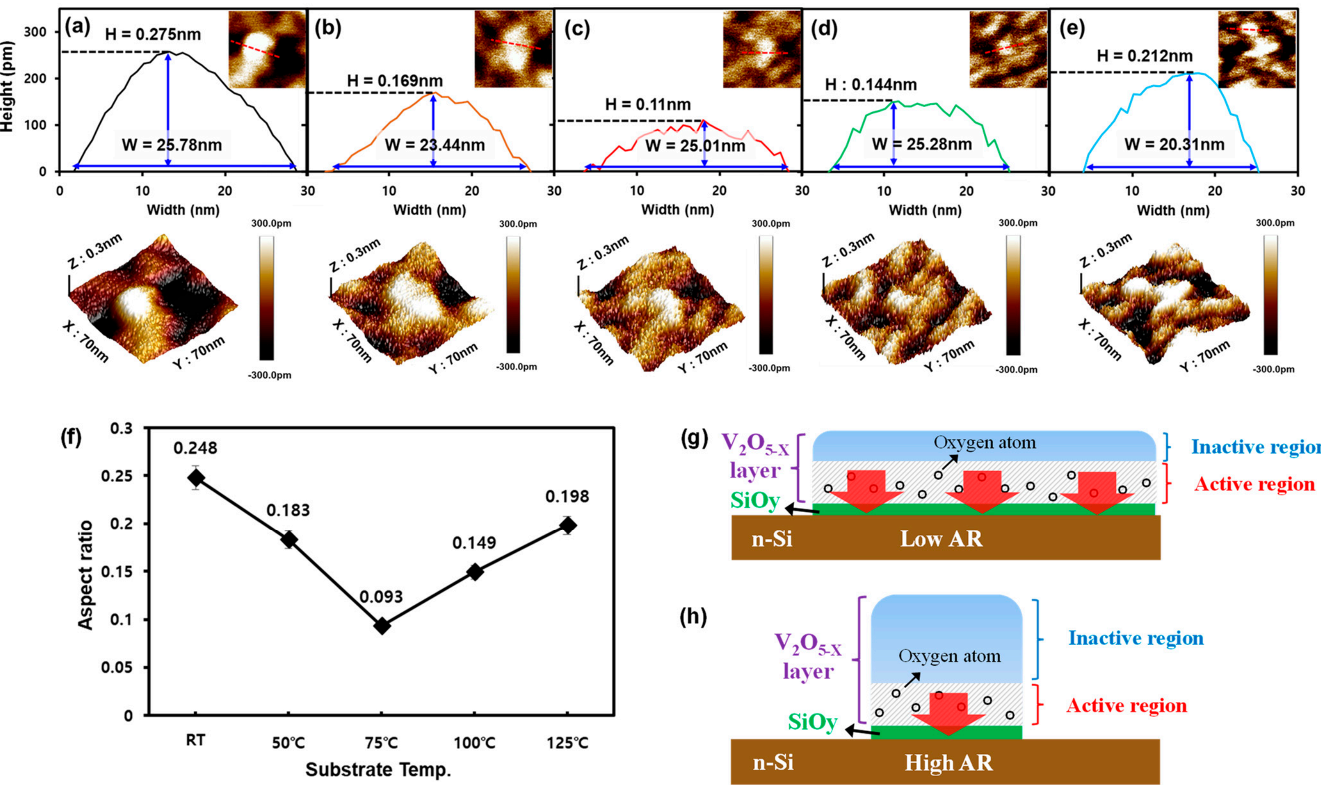

Figure 6. AFM images measured in 3D, and height and width of V_2O_{5-x} islands at (**a**) RT, (**b**) 50 °C, (**c**) 75 °C, (**d**) 100 °C, and (**e**) 125 °C; (**f**) calculated aspect ratios (ARs). Schematic of the effect of the AR on the surface area of SiO_y for (**g**) low-AR and (**h**) high-AR V_2O_{5-x} islands.

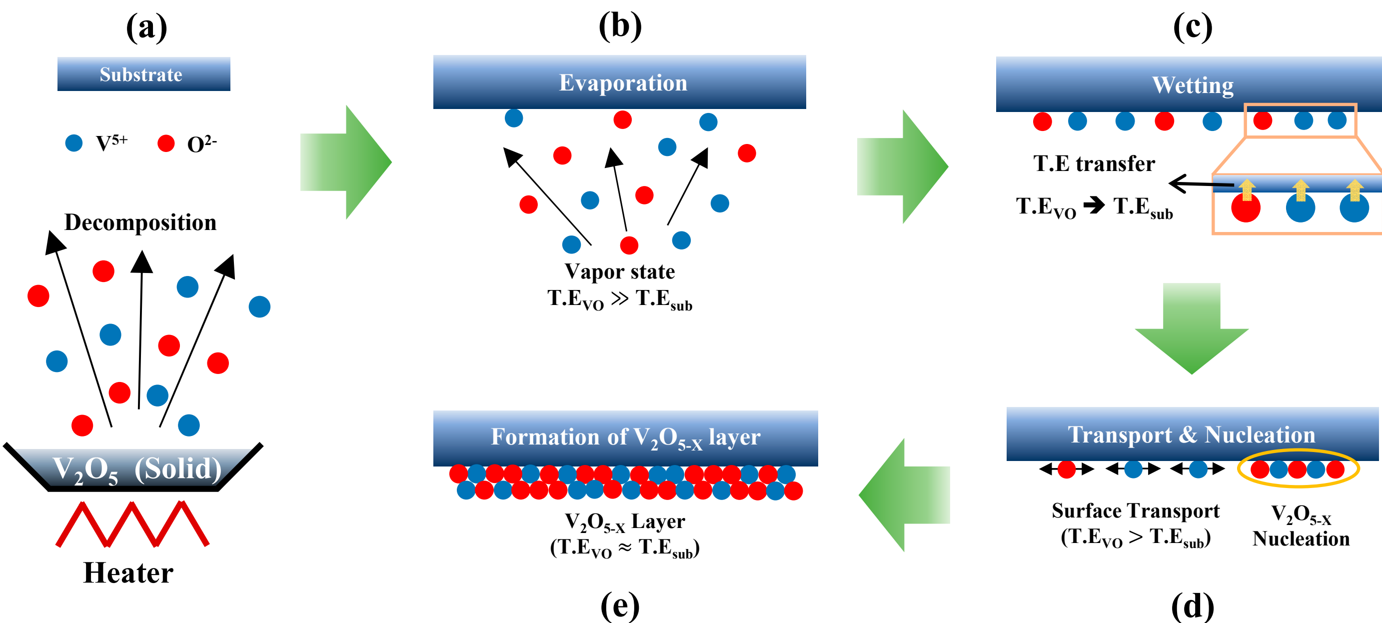

Figure 7. Schematic illustration of the solid-state V_2O_{5-x} TF formation processes. (**a**) crucible heating (**b**) material evaporation (**c**) substrate wetting (**d**) surface transport and nucleation and (**e**) formation of V_2O_{5-x} layer.

In this process, assuming that the operating power, deposition distance, and vacuum conditions are the same, then the quality of the TF in terms of the stoichiometry, uniformity, and coverage would be most significantly affected by the distance the atoms are transported and the V_2O_{5-x} nucleation rate on the surface in Figure 7d [39,40]. Based on this consideration, the observed AR variation with the deposition temperature can be explained by (1) the distance the atoms are transported and (2) nucleation rate. First, in terms of the transportation distance of the atoms, at low substrate temperatures, the amount of TE transferred from the atoms to the substrate would be relatively large to achieve thermal equilibrium between TE_{VO} and TE_{sub}. This would result in the rapid adsorption of V and O atoms onto the surface when they reach the substrate, but the distance the atoms are transported would decrease owing to excessive TE loss. Therefore, at low substrate temperatures, the AR of the V_2O_{5-x} islands would be expected to be high. In contrast, at higher substrate temperatures, TE transfer from the atoms to the substrate decreases. Hence, the depositing atoms could be transported for a comparatively longer distance, which would lower the AR of the V_2O_{5-x} islands. However, as presented in Figure 6f, the AR of the V_2O_{5-x} islands gradually decreased only until 75 °C, after which it increased again at higher temperatures (i.e., 100 and 125 °C). On the basis of this behavior, we assume that the nucleation rate for the V_2O_{5-x} would decrease at temperatures above 75 °C, at which more metallic V-rich V_2O_{5-x} islands would form to increase the AR [40,41]. To confirm this assumption, additional XPS measurements were performed to investigate the stoichiometry of the V_2O_{5-x} TFs deposited at different temperatures and the results are presented in Figures 8 and 9. The results confirmed that deposition temperature notably affected the composition of the vanadium oxidation states (VOS) in the deposited V_2O_{5-x} TFs.

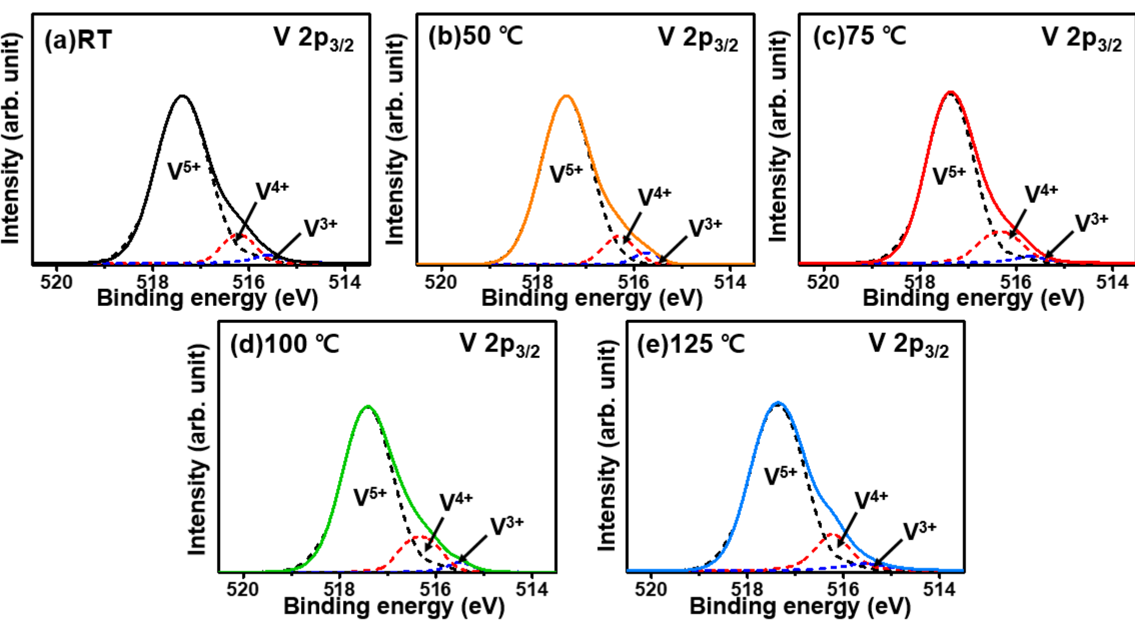

Figure 8. V $2p_{3/2}$ XPS profiles of V_2O_{5-x} (15 nm) TFs deposited on Si surfaces at various deposition temperatures: (**a**) RT, (**b**) 50 °C, (**c**) 75 °C, (**d**) 100 °C, and (**e**) 125 °C.

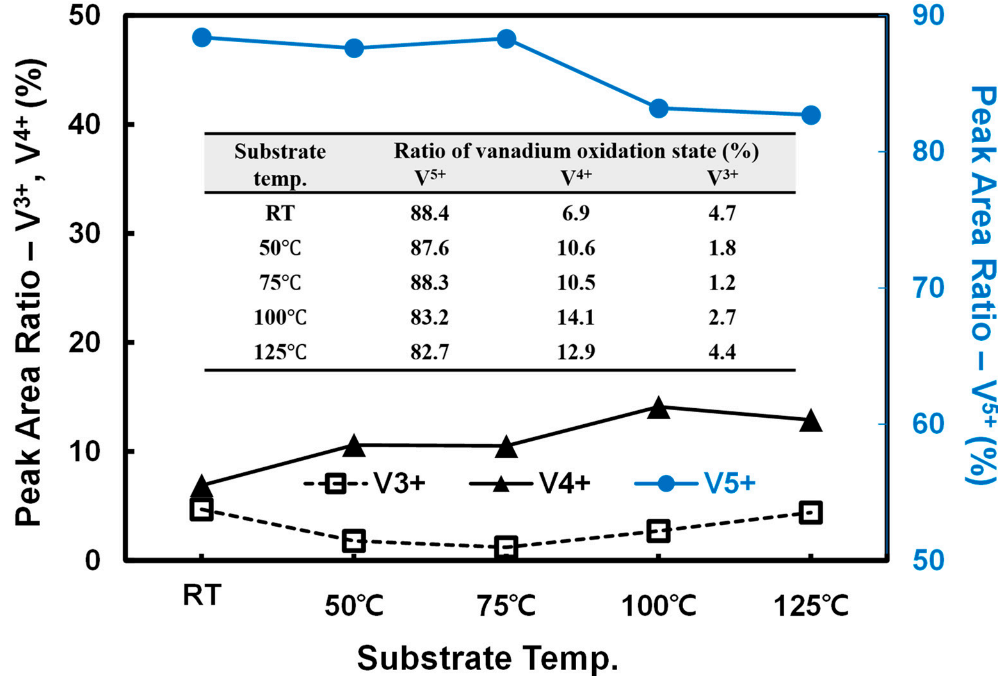

Substrate temp.	Ratio of vanadium oxidation state (%)		
	V5+	V4+	V3+
RT	88.4	6.9	4.7
50°C	87.6	10.6	1.8
75°C	88.3	10.5	1.2
100°C	83.2	14.1	2.7
125°C	82.7	12.9	4.4

Figure 9. Integrated peak area ratios of vanadium oxidation states based on the measured V 2p XPS profiles.

In Figure 8, the V 2p XPS results exhibit no change in the peak positions at the tested temperatures; the peaks are assigned to V_2O_{5-x}. Figure 8 shows that the deposition of V_2O_{5-x} on Si occurs via the formation of various VOS, identified as V^{5+} with a high binding energy, and V^{4+} and V^{3+} with lower binding energies, respectively [7,42,43]. The measured XPS profiles were deconvoluted to distinguish the individual VOS within the V_2O_{5-x} TFs, followed by calculation of the peak areas to compare the composition ratios of the three VOS, namely, V^{5+}, V^{4+}, and V^{3+} (Figure 9). The results from the Figure 9 showed that, as the deposition temperature increases from RT to 75 °C, the ratio of V^{5+} is preserved at

approximately 88%, whereas that of V^{4+} increases from 6.9% to 10.5%. With respect to V^{3+}, the increase in the V^{4+} state likely arises from the decrease in the ratio of the V^{3+} state from 4.7% at RT to 1.2% at 75 °C, seemingly as a result of the oxidation of V^{3+} to V^{4+}.

However, as the deposition temperature increases to 100 °C, the V^{5+} state, which remained at approximately 88% of the VOS up to 75 °C, sharply decreased to 83% at higher temperatures. Simultaneously, the ratio of V^{4+} increased from 10.5% to 14.1%, and that of V^{3+}, from 1.2% to 2.7%. Thus, the VOS in the TF underwent reduction to lower states. This trend was more pronounced when the deposition temperature was increased to 125 °C. This implies that the nucleation of V_2O_{5-x} above 75 °C is limited because of its high temperature [40]. Therefore, as indicated in Figure 9 and the embedded table, the ratio of lower VOS would increase as a result of the significant loss of volatile O atoms from the surface followed by the formation of V_2O_{5-x} islands with high AR, as shown in Figure 6.

With these results, we demonstrated that the optimal deposition temperature can promote the passivation capability of the deposited V_2O_{5-x} TF owing to the effective formation of the SiO_y layer at the V_2O_{5-x}/Si interface because of the low AR of the initial V_2O_{5-x} islands. However, this facilitated formation of SiO_y could also improve the electrical conductivity of the V_2O_{5-x} TF itself by inducing the generation of O deficiencies in the V_2O_{5-x} TF [25,44]. Therefore, using the TLM, the electrical conductivities were also measured as a function of the deposition temperature, and the results are shown in Figure S1. The electrical conductivities measured above 75 °C were higher compared to those at lower temperatures and this was mostly attributed to the higher occurrence of lower VOS within the V_2O_{5-x} TFs above 75 °C.

Finally, the relationship between the V_2O_{5-x} deposition temperature and the performance of the solar cell was investigated by fabricating Si/V_2O_{5-x} HSCs at different substrate temperatures, as shown in Figure 10. Figure 8b shows the current density vs. voltage (J–V) curve for the fabricated HSCs, and Table 1 summarizes the HSC performance parameters. These results clearly confirmed that the HSC fabricated at 75 °C had the highest PCE value of 3.3%, compared to those fabricated at the other temperatures. As is clear from Table 1, the overall solar cell performance of the HSC fabricated at 75 °C is higher compared to that at the other temperatures. Most notably, in terms of FF, the 75 °C sample had the highest value of 37.8%. For the Si-based solar cell, effective passivation on high defect states on the surface is crucial to improve R_{sh}. In addition, providing reduced sheet resistance of contact layers is also highly important to decrease R_s. Therefore, as shown in Figure 2 and Figure S1, the enhanced passivation effect at 75 °C and improved V_2O_{5-x} conductivity were the main factors for the improve PCE with the 75 °C sample [45,46]. However, the morphology of the V_2O_{5-x} TF presumably also affected the value of R_s considering that the smoothest surface morphology was produced at 75 °C, thereby improving the metal contact resistance in the HSCs.

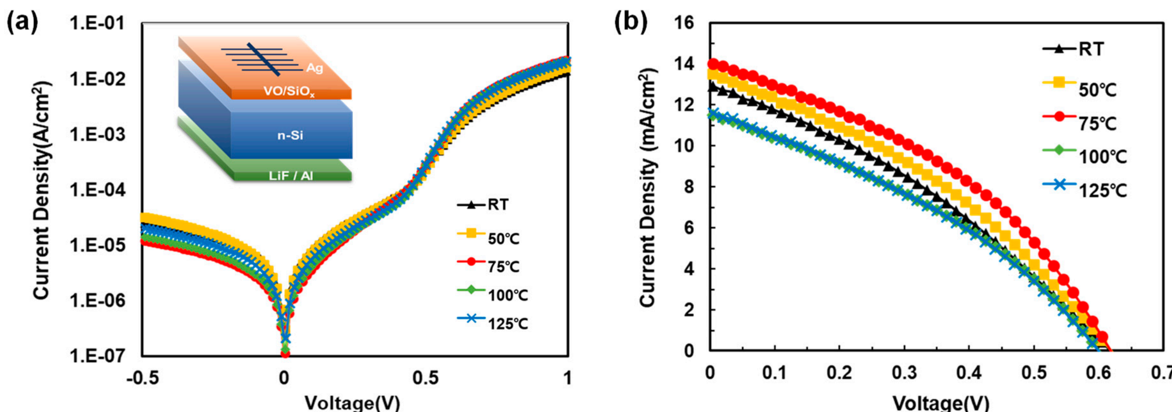

Figure 10. Current density vs. voltage curves of Si/V_2O_{5-x} HSCs measured under (**a**) dark and (**b**) 100 mW/cm^2 illumination (AM1.5) conditions.

Table 1. Solar cell performance parameters of Si/V_2O_{5-x} HSCs.

Substrate Temp.	J_{sc} (mA/cm^2)	V_{oc} (mV)	FF (%)	R_{sh} ($\Omega\cdot$cm^2)	R_s ($\Omega\cdot$cm^2)	PCE (%)
RT	12.98	618	32.85	13027	7.20	2.63
50 °C	13.51	619	34.72	13574	6.01	2.90
75 °C	14.09	618	37.81	14122	5.65	3.29
100 °C	11.54	601	34.63	11583	7.18	2.40
125 °C	11.64	600	34.23	11693	7.60	2.39

4. Conclusions

In this report, we presented our systematic comparative study to explore the effect of the deposition temperature on the ability of the V_2O_{5-x} TF to passivate the Si surface. Our results confirmed that the τ_{eff} can be considerably enhanced even with a minor elevation in the temperature at which the V_2O_{5-x} TF is deposited below 100 °C. The XPS measurements showed that formation of the SiO_x passivation layer at the Si/V_2O_{5-x} interface is highly facilitated even at a temperature as low as 75 °C, which is an unprecedentedly low temperature for TMO thermal treatment in general. To investigate the origin of the improved passivation effect at such a low temperature, the morphologies of the initial V_2O_{5-x} islands were analyzed. The AR of the V_2O_{5-x} islands was found to be highly sensitive to even minor changes in the deposition temperature below 125 °C. In addition, a detailed study of the VOS with XPS revealed that the stoichiometry of the V_2O_{5-x} TF was also notably affected by the deposition temperature. Consequently, a specific temperature, 75 °C, was found to produce V_2O_{5-x} islands with the lowest AR, which offers the most-expanded V_2O_{5-x}-active region to supply O atoms to the Si surface for effective SiO_y layer formation. As a result, the PCE of fabricated Si/V_2O_{5-x} HSCs was noticeably higher at our optimized deposition temperature compared to the PCE of the other HSCs.

Supplementary Materials: The following supporting information can be downloaded at: https://www.mdpi.com/article/10.3390/ma15155243/s1, Figure S1: (a) Measured sheet resistance of VO TFs according to Si substrate temperature extracted from the ohmic current-voltage response in TLM measurements and (b) derived conductivities of each VO TFs; Figure S2: Experimental Mott-Schottky plots and linear fittings for the samples from the different deposition temperature. Reference [47] are cited in the supplementary materials.

Author Contributions: Data curation, Y.-C.J.; Formal analysis, G.S.J.; Funding acquisition, J.-Y.C.; Investigation, G.S.J.; Methodology, Y.-C.J., N.Y.P., Y.-J.Y., J.H.L. and J.H.S.; Project administration, J.-Y.C.; Resources, J.-Y.C.; Visualization, N.Y.P., J.H.L. and J.H.S.; Writing–original draft, G.S.J.; Writing–review & editing, J.-Y.C. All authors have read and agreed to the published version of the manuscript.

Funding: This work was supported by a grant from the National Research Foundation of Korea (NRF) funded by the Korean government (Ministry of Science and ICT) (2020R1F1A1053556).

Conflicts of Interest: The authors declare no conflict of interest.

References

1. Louwen, A.; Van Sark, W.; Schropp, R.; Faaij, A. A cost roadmap for silicon heterojunction solar cells. *Sol. Energy Mater. Sol. Cells* **2016**, *147*, 295–314. [CrossRef]
2. Bermel, P.; Luo, C.; Zeng, L.; Kimerling, L.C.; Joannopoulos, J.D. Improving thin-film crystalline silicon solar cell efficiencies with photonic crystals. *Opt. Express* **2007**, *15*, 16986–17000. [CrossRef] [PubMed]
3. Chong, T.K.; Wilson, J.; Mokkapati, S.; Catchpole, K.R. Optimal wavelength scale diffraction gratings for light trapping in solar cells. *J. Opt.* **2012**, *14*, 024012. [CrossRef]
4. Hwang, I.; Jeong, Y.; Shiratori, Y.; Park, J.; Miyajima, S.; Yoon, I.; Seo, K. Effective Photon Management of Non-Surface-Textured Flexible Thin Crystalline Silicon Solar Cells. *Cell Rep. Phys. Sci.* **2020**, *1*, 100242.
5. Zhang, Y.; Stokes, N.; Jia, B.; Fan, S.; Gu, M. Towards ultra-thin plasmonic silicon wafer solar cells with minimized efficiency loss. *Sci. Rep.* **2014**, *4*, 4393. [CrossRef]
6. Werner, J.; Niesen, B.; Ballif, C. Perovskite/silicon tandem solar cells: Marriage of convenience or true love story?—An overview. *Adv. Mater. Interfaces* **2018**, *5*, 1700731. [CrossRef]

7. Wu, Q.-H.; Thissen, A.; Jaegermann, W.; Liu, M. Photoelectron spectroscopy study of oxygen vacancy on vanadium oxides surface. *Appl. Surf. Sci.* **2004**, *236*, 473–478. [CrossRef]
8. Weingarten, M.; Zweipfennig, T.; Vescan, A.; Kalisch, H. Low-temperature processed hybrid organic/silicon solar cells with power conversion efficiency up to 6.5%. *MRS Online Proc. Libr. Arch.* **2015**, *1771*, 201–206. [CrossRef]
9. Thomas, J.P.; Leung, K.T. Defect-minimized PEDOT: PSS/planar-Si solar cell with very high efficiency. *Adv. Funct. Mater.* **2014**, *24*, 4978–4985. [CrossRef]
10. Hussain, B.; Ebong, A.; Ferguson, I. Zinc oxide as an active n-layer and antireflection coating for silicon based heterojunction solar cell. *Sol. Energy Mater. Sol. Cells* **2015**, *139*, 95–100. [CrossRef]
11. Bivour, M.; Temmler, J.; Steinkemper, H.; Hermle, M. Alternative contact materials for induced junction silicon solar cells. *Sol. Energy Mater. Sol. Cells* **2015**, *142*, 34–41. [CrossRef]
12. Bullock, J.; Yan, D.; Cuevas, A.; Wan, Y.; Samundsett, C. N-and p-typesilicon solar cells with molybdenum oxide hole contacts. *Energy Procedia* **2015**, *77*, 446–450. [CrossRef]
13. Smith, R.P.; Hwang, A.A.-C.; Beetz, T.; Helgren, E. Introduction to semiconductor processing: Fabrication and characterization of pn junction silicon solar cells. *Am. J. Phys.* **2018**, *86*, 740–746. [CrossRef]
14. He, J.; Wang, G.; Qiu, Y.; Tang, Z.; Ye, F.; Zhang, C.; Wang, S.; Cai, L.; Yu, T.; Gao, P. Enabling Transparent-Conductive-Oxide Free Efficient Heterojunction Solar Cells by Flexibly Using Dopant-Free Contact. *Adv. Funct. Mater.* **2022**, 2205901. [CrossRef]
15. Meyer, J.; Hamwi, S.; Kröger, M.; Kowalsky, W.; Riedl, T.; Kahn, A. Transition metal oxides for organic electronics: Energetics, device physics and applications. *Adv. Mater.* **2012**, *24*, 5408–5427. [CrossRef]
16. Gerling, L.G.; Mahato, S.; Voz, C.; Alcubilla, R.; Puigdollers, J. Characterization of transition metal oxide/silicon heterojunctions for solar cell applications. *Appl. Sci.* **2015**, *5*, 695–705. [CrossRef]
17. Cho, E.-C.; Cho, Y.H.; Yi, J. Research and Development Trend of Carrier Selective Energy Contact Solar Cells. *Curr. Photovolt. Res.* **2018**, *6*, 43–48.
18. Wang, Z.; Li, P.; Liu, Z.; Fan, J.; Qian, X.; He, J.; Peng, S.; He, D.; Li, M.; Gao, P. Hole selective materials and device structures of heterojunction solar cells: Recent assessment and future trends. *APL Mater.* **2019**, *7*, 110701. [CrossRef]
19. Wu, W.; Bao, J.; Jia, X.; Liu, Z.; Cai, L.; Liu, B.; Song, J.; Shen, H. Dopant-free back contact silicon heterojunction solar cells employing transition metal oxide emitters. *Phys. Status Solidi (RRL)–Rapid Res. Lett.* **2016**, *10*, 662–667. [CrossRef]
20. Hussain, S.Q.; Mallem, K.; Kim, Y.J.; Le, A.H.T.; Khokhar, M.Q.; Kim, S.; Dutta, S.; Sanyal, S.; Kim, Y.; Park, J. Ambient annealing influence on surface passivation and stoichiometric analysis of molybdenum oxide layer for carrier selective contact solar cells. *Mater. Sci. Semicond. Process.* **2019**, *91*, 267–274. [CrossRef]
21. Tong, J.; Wan, Y.; Cui, J.; Lim, S.; Song, N.; Lennon, A. Solution-processed molybdenum oxide for hole-selective contacts on crystalline silicon solar cells. *Appl. Surf. Sci.* **2017**, *423*, 139–146. [CrossRef]
22. Wang, F.; Tan, Z.a.; Li, Y. Solution-processable metal oxides/chelates as electrode buffer layers for efficient and stable polymer solar cells. *Energy Environ. Sci.* **2015**, *8*, 1059–1091. [CrossRef]
23. Geissbühler, J.; Werner, J.; Martin de Nicolas, S.; Barraud, L.; Hessler-Wyser, A.; Despeisse, M.; Nicolay, S.; Tomasi, A.; Niesen, B.; De Wolf, S. 22.5% efficient silicon heterojunction solar cell with molybdenum oxide hole collector. *Appl. Phys. Lett.* **2015**, *107*, 081601. [CrossRef]
24. Yu, C.; Xu, S.; Yao, J.; Han, S. Recent advances in and new perspectives on crystalline silicon solar cells with carrier-selective passivation contacts. *Crystals* **2018**, *8*, 430. [CrossRef]
25. Gerling, L.G.; Voz, C.; Alcubilla, R.; Puigdollers, J. Origin of passivation in hole-selective transition metal oxides for crystalline silicon heterojunction solar cells. *J. Mater. Res.* **2017**, *32*, 260–268. [CrossRef]
26. Yang, X.; Zheng, P.; Bi, Q.; Weber, K. Silicon heterojunction solar cells with electron selective TiOx contact. *Sol. Energy Mater. Sol. Cells* **2016**, *150*, 32–38. [CrossRef]
27. Liang, Z.; Su, M.; Zhou, Y.; Gong, L.; Zhao, C.; Chen, K.; Xie, F.; Zhang, W.; Chen, J.; Liu, P. Interaction at the silicon/transition metal oxide heterojunction interface and its effect on the photovoltaic performance. *Phys. Chem. Chem. Phys.* **2015**, *17*, 27409–27413. [CrossRef]
28. Gerling, L.G.; Masmitja, G.; Ortega, P.; Voz, C.; Alcubilla, R.; Puigdollers, J. Passivating/hole-selective contacts based on V2O5/SiOx stacks deposited at ambient temperature. *Energy Procedia* **2017**, *124*, 584–592. [CrossRef]
29. Bergerud, A.J. *Phase Stability and Transformations in Vanadium Oxide Nanocrystals*; University of California: Berkeley, CA, USA, 2016.
30. Neudeck, G.W.; Pierret, R.F. Introduction to microelectronic fabrication. *Modul. Ser. Solid State Devices* **2002**, *5*, 57–65.
31. Zhang, W.L.; Zhang, S.; Yang, M.; Chen, T.P. Microstructure of Magnetron Sputtered Amorphous SiO x Films: Formation of Amorphous Si Core− Shell Nanoclusters. *J. Phys. Chem. C* **2010**, *114*, 2414–2420. [CrossRef]
32. Lisovskyy, I.; Voitovych, M.; Sarikov, A.; Litovchenko, V.; Romanyuk, A.; Melnyk, V.; Khatsevich, I.; Shepeliavyi, P.; Lashkarev, V. Transformation of the structure of silicon oxide during the formation of Si nanoinclusions under thermal annealings. *Ukr. J. Phys.* **2009**, *54*, 383–390.
33. Ali, H.; Koul, S.; Gregory, G.; Bullock, J.; Javey, A.; Kushima, A.; Davis, K.O. Thermal stability of hole-selective tungsten oxide: In situ transmission electron microscopy study. *Sci. Rep.* **2018**, *8*, 12651. [CrossRef] [PubMed]
34. Ferrari, M.; Liggieri, L.; Miller, R. *Drops and Bubbles in Contact with Solid Surfaces*; CRC Press: Boca Raton, FL, USA, 2012.
35. Shafrin, E.G.; Zisman, W. Effect of temperature on wetting of high-and low-energy solid surfaces. *J. Phys. Chem.* **1972**, *76*, 3259–3267. [CrossRef]

36. Ritala, M.; Leskelä, M. Atomic layer deposition. In *Handbook of Thin Films*; Elsevier: Amsterdam, The Netherlands, 2002; pp. 103–159.
37. Abegunde, O.O.; Akinlabi, E.T.; Oladijo, O.P.; Akinlabi, S.; Ude, A.U. Overview of thin film deposition techniques. *AIMS Mater. Sci.* **2019**, *6*, 174–199. [CrossRef]
38. Hora, J.; Hall, C.; Evans, D.; Charrault, E. Inorganic thin film deposition and application on organic polymer substrates. *Adv. Eng. Mater.* **2018**, *20*, 1700868. [CrossRef]
39. Barote, M.; Yadav, A.; Masumdar, E. Effect of deposition parameters on growth and characterization of chemically deposited Cd1-XPbXS thin films. *Chalcogenide Lett.* **2011**, *8*, 129–138.
40. Elam, J.W.; Baker, D.A.; Hryn, A.J.; Martinson, A.B.; Pellin, M.J.; Hupp, J.T. Atomic layer deposition of tin oxide films using tetrakis (dimethylamino) tin. *J. Vac. Sci. Technol. A Vac. Surf. Film.* **2008**, *26*, 244–252. [CrossRef]
41. Sarkar, T.; Ghosh, S.; Annamalai, M.; Patra, A.; Stoerzinger, K.; Lee, Y.-L.; Prakash, S.; Motapothula, M.R.; Shao-Horn, Y.; Giordano, L. The effect of oxygen vacancies on water wettability of transition metal based $SrTiO_3$ and rare-earth based Lu_2O_3. *RSC Adv.* **2016**, *6*, 109234–109240. [CrossRef]
42. Zhao, X.; Yan, Y.; Mao, L.; Fu, M.; Zhao, H.; Sun, L.; Xiao, Y.; Dong, G. A relationship between the V_{4+}/V_{5+} ratio and the surface dispersion, surface acidity, and redox performance of V_2O_5–WO_3/TiO_2 SCR catalysts. *RSC Adv.* **2018**, *8*, 31081–31093. [CrossRef]
43. Lim, C.J.; Park, M.G.; Kim, M.S.; Han, J.H.; Cho, S.; Cho, M.-H.; Yi, Y.; Lee, H.; Cho, S.W. Electronic structure of C60/zinc phthalocyanine/V_2O_5 interfaces studied using photoemission spectroscopy for organic photovoltaic applications. *Molecules* **2018**, *23*, 449. [CrossRef]
44. Shewchun, J.; Singh, R.; Green, M. Theory of metal-insulator-semiconductor solar cells. *J. Appl. Phys.* **1977**, *48*, 765–770. [CrossRef]
45. Sun, T.; Wang, R.; Liu, R.; Wu, C.; Zhong, Y.; Liu, Y.; Wang, Y.; Han, Y.; Xia, Z.; Zou, Y. Investigation of MoOx/n-Si strong inversion layer interfaces via dopant-free heterocontact. *Phys. Status Solidi (RRL)–Rapid Res. Lett.* **2017**, *11*, 1700107. [CrossRef]
46. Dauwe, S.; Mittelstädt, L.; Metz, A.; Hezel, R. Experimental evidence of parasitic shunting in silicon nitride rear surface passivated solar cells. *Prog. Photovolt. Res. Appl.* **2002**, *10*, 271–278. [CrossRef]
47. Almora, O.; Gerling, L.G.; Voz, C.; Alcubilla, R.; Puigdollers, J.; Garcia-Belmonte, G. Superior performance of V_2O_5 as hole selective contact over other transition metal oxides in silicon heterojunction solar cells. *Sol. Energy Mater. Sol. Cells* **2017**, *168*, 221–226. [CrossRef]